Melt in Antarctica derived from SMOS observations at L band

Marion Leduc-Leballeur[1], Ghislain Picard[2], Giovanni Macelloni[1], Arnaud Mialon[3], and Yann K. Kerr[3]

[1]Institute of Applied Physics "Nello Carrara" – National Council of Research, 50019 Sesto Fiorentino, Italy
[2]UGA, CNRS, Institut des Géosciences de l'Environnement (IGE), UMR 5001, Grenoble, 38041, France
[3]CESBIO (CNES, CNRS, IRD, UPS), Univ. Toulouse, 31401 Toulouse Cedex 09, France

Correspondence: Leduc-Leballeur (m.leduc@ifac.cnr.it)

Abstract. Melt occurrence in Antarctica is derived from L-band observations from the Soil Moisture and Ocean Salinity (SMOS) satellite between the austral summer 2010/11 and 2017/18. The detection algorithm is adapted from a threshold method previously developed for 19 GHz passive microwave measurements from Special Sensor Microwave Imagers (SSM/I, SSMIS). The comparison of daily melt occurrence retrieved from 1.4 GHz and 19 GHz observations shows an overall close
5 agreement, but a lag of few days is usually observed by SMOS at the beginning of the melt season. To understand the difference, we performed a theoretical analysis using a microwave emission radiative transfer model that shows that the sensitivity of 1.4 GHz signal to liquid water is significantly weaker than at 19 GHz if the water is only present in the uppermost tens of centimeters of the snowpack. Conversely, 1.4 GHz measurements are sensitive to water when spread over at least 1 m and when present at depth, up to hundreds of meters. This is explained by the large penetration depth in dry snow and by
10 the long wavelength (21 cm). We conclude that SMOS and higher frequency radiometers provide interesting complementary information on melt occurrence and on the location of the water in the snowpack.

1 Introduction

Melt occurs in coastal Antarctica and on ice shelves during the austral summer. Its duration and extent are useful climate indicators due to their connection to surface temperature and surface energy budget (e.g. Liu et al., 2006; Picard et al., 2007).
15 Moreover, intense melting event has been identified as a precursor of some major ice shelf collapses (Scambos et al., 2000). Thus, monitoring of the melt season contributes to characterize the seasonal and inter-annual climatic variations in Antarctica and is important to assess the future stability of the ice-sheet (Golledge et al., 2015).

Remote sensing offers a particularly relevant means to obtain information over the entire Antarctic continent and over long-term periods, given the very rare in situ measurements related to melt or liquid water (Jakobs et al., 2019). Microwave
20 radiometers have been widely used to detect melt in polar regions exploiting the marked increase of brightness temperature due to the high absorption of microwaves by water relative to that of dry snow. Various detection algorithms have been developed and applied in Greenland (e.g. Mote et al., 1993; Abdalati and Steffen, 1997; Tedesco, 2007) and Antarctica (e.g. Ridley, 1993; Zwally and Fiegles, 1994; Torinesi et al., 2003; Liu et al., 2005, 2006; Tedesco et al., 2007). They have mainly used 19 GHz and 37 GHz frequencies available since 1979 from several satellite sensors such as the Scanning Multichannel Microwave Radiometer (SMMR) on the Nimbus 7 satellite or the Special Sensor Microwave/Imager (SSM/I) and Special Sensor

Microwave Imager Sounder (SSMIS) from the Defense Meteorological Satellite Program (DMSP) satellites. Since 2009, the Soil Moisture and Ocean Salinity (SMOS) satellite has provided radiometric observations at L band (1.4 GHz), a frequency capable of penetrating much deeper in the ice sheets, on the order of several hundred meters at 1.4 GHz (Passalacqua et al., 2018) compared to only a few meters for the higher frequencies (Surdyk, 2002). This suggests that L-band observations could

30   offer new information on melt.

The aim of this study is to retrieve melt in Antarctica from daily SMOS observations, and to investigate the similarities and differences with melt detected at 19 GHz. Section 2 introduces the data sets. Section 3 describes the method to detect melt and Section 4 compares the daily melt occurrence obtained with 1.4 GHz and 19 GHz observations. Section 5 presents a modeling study to assess the liquid water sensitivity of brightness temperature (T_B) at 1.4 GHz and to discuss the differences

35   with 19 GHz.

2 Data sets

2.1 SMOS observations

The SMOS mission was developed by the European Space Agency (ESA) in collaboration with the Centre National d'Etudes Spatiales (CNES) in France and the Centro para el Desarrollo Tecnologico Industrial (CDTI) in Spain. This satellite is operated

40   by CNES and ESA and carries on board a L-band interferometric radiometer operating at 1.4 GHz (21 cm) with an averaged ground resolution of 43 km(Kerr et al., 2010). The radiometer provides multi-angular fully polarized T_B (Kerr et al., 2001).

The SMOS Level 3 product delivers multi-angular T_B at top of the atmosphere in the antenna polarization reference frame (Al Bitar et al., 2017). The product is georeferenced on the Equal-Area Scalable Earth version 2.0 grid (EASE–Grid 2; Brodzik et al. (2012)), with an over-sampled resolution of about 628 km^2, which is distorted in the polar regions (around 100×6 km^2

45   as latitude×longitude). It comprises daily-average and incident angle-average with angle bins every 5º from 0º to 65º. T_B at vertical (V) and horizontal (H) polarizations at 52.5º of incidence angle are used here. They come from the RE04 reprocessed version between April 2010 and April 2015, and from operational version between Mai 2015 to March 2019, both distributed by CATDS (Centre Aval de Traitement des Données SMOS; www.catds.fr).

The gaps shorter than 3 days in the SMOS time series are filled by a linear interpolation. Longer gaps result in missing value

50   in the product. If more than 60 days are missing over a year, the grid point is ignored for that year (about 7% of pixel every year, mainly south of 83ºS).

2.2 Observations at 19 GHz and daily surface melting

Satellite observations at 19 GHz were acquired by the Special Sensor Microwave/Imager (SSM/I) and Special Sensor Microwave Imager Sounder (SSMIS), processed by the National Snow and Ice Data Center (NSIDC, Maslanik and Stroeve

55   (2004, updated 2018)).

Daily T_B observations at H polarization are processed according to Picard and Fily (2006); Picard et al. (2007) to derive daily surface melt from 1979 to 2018 (data available from http://gp.snow-physics.science/melting). This data set provides daily melt status, i.e. presence or absence of liquid water, for every grid point on the Southern stereographic polar grid with a grid spacing of 25 km^2. The effective resolution of the product is coarser, of the order of 40 km, close to that provided by SMOS.

3 Melting detection method

The algorithm to detect melt occurrence from the 1.4 GHz observations is inspired by the work at 19 GHz of Torinesi et al. (2003), itself based on Zwally and Fiegles (1994). The algorithm determines an optimal threshold for every year in every pixel, and considers that any daily T_BH over this threshold indicate melting occurrence. T_B is measured at large observation angle (above 50°). In this configuration, the H polarization is favored because the emissivity of dry firn is usually significantly lower at H than at V polarization, while the emissivity of wet firn is always close to 1 at both polarizations. It results that the increase in T_B from dry to wet snow is more significant at H polarization, and easier to detect.

The algorithm uses an adaptive threshold T in each grid point and for each year given by $T = M + a\sigma$, with M the time average and σ the standard deviation of T_B when snow is dry. According to the analysis of daily air surface temperature, Torinesi et al. (2003) found a suitable value of $a = 3$ so that most melting events correspond to daily maximum temperatures above -5°C. This value is also typical for outliers detection (e.g. von Storch and Zwiers, 2001).

To solve the circular problem of computing M and σ for non melting days in order to detect melting days, the initial step consists in calculating M in each grid point on a fixed period of one year – from 1 April to 31 March – and in setting $a\sigma$ to a first-guess fixed value. Previous studies for 19 GHz used $a\sigma = 30$ K. However, we found it unsuitable at 1.4 GHz, because of the weaker sensitivity to liquid water (Section 5). We instead propose a lower first guess value of $a\sigma = 15$ K.

With these assumptions, a first guess melt time series is detected and new estimates of M and σ are computed by removing melting days from the T_B series, still limiting the period from 1 April and 31 March. Melt is then detected once again using the updated threshold. The process is iterated three times to ensure stable estimates. The algorithm returns a binary indicator for each day and each grid point, 0 for the absence and 1 for the present of liquid water.

This algorithm needs further correction for some false alarms found on the Antarctic Plateau where melt is known to never occur. These alarms are likely due to variations of T_BH of the order of several Kelvin that were reported by Brucker et al. (2014) and Leduc-Leballeur et al. (2017) and explained to result from the snow metamorphism and surface hoar removal by wind storms. Noting that these changes do not impact T_BV, although melt does, we consider here that the areas with low annual standard deviation of T_BV are not subject to melt. We estimated a threshold standard deviation of 2.8 K based on the fact that it excludes 95 % of grid points with surface elevation higher than 1500 m. Thus, as a final step of the algorithm, the grid points with a T_BV annual standard deviation lower than this threshold are masked out that year.
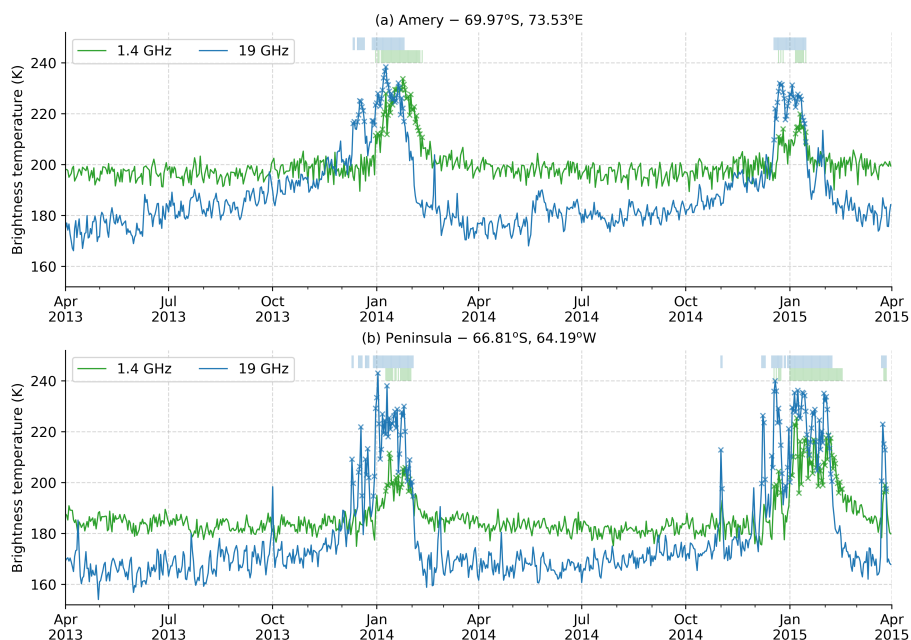
Figure 1. Brightness temperature at H polarization (K) at 1.4 GHz (green) and 19 GHz (blue) from April 2012 to March 2014 on (a) the Amery area and (b) the Antarctic Peninsula. The melting days detected by each frequency are depicted by crosses on the time series and recalled by pale lines above.

4   Comparison with 19 GHz

Figure 1 shows two examples of two consecutive melt seasons in the Amery area (69.97ºS, 73.53ºE) and the Antarctic Peninsula (66.81ºS, 64.19ºW). For each event, melt is detected several days earlier at 19 GHz compared to 1.4 GHz. For instance, in 11 December 2013 on the Amery time series, a short melting event lasting 6 days is missed at 1.4 GHz while it is well detected at 19 GHz. This suggests that this event was weak and only affected the superficial part of the snowpack. On the other hand, the short melting event during March 2015 on the Peninsula time series is detected by both frequencies, suggesting intense melt with percolation in a large upper part of the snowpack.

The beginning of the melt season detected usually largely differs between both frequencies as illustrated in Figure 2. On average, the first melting day can be detected as early as September at 19 GHz, while it is rare to detect melt earlier than December at 1.4 GHz. For the pixel where melt is detected by both frequencies in a given year, the 19 GHz detection precedes by 1-5 days for 28% of the pixels and by 6-15 days for 26% of them. This lag is also observed for the end of the season with a remanence of the melt detected at 1.4 GHz until nearly April.

Figure 2 also highlights that the melt extent detected at 19 GHz is 3 to 6 times as large as at 1.4 GHz, depending on the years. The standard deviation maximum is reached in January at 250,000 km^2 and 110,000 km^2 for 19 GHz and 1.4 GHz, respectively.
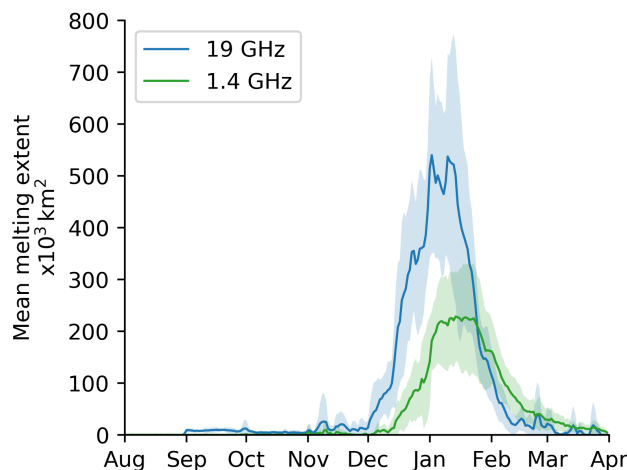
Figure 2. Daily mean melting extent from April 2010 to March 2018 detected with observations at 1.4 GHz (green) and at 19 GHz (blue). Standard deviation is in pale area.
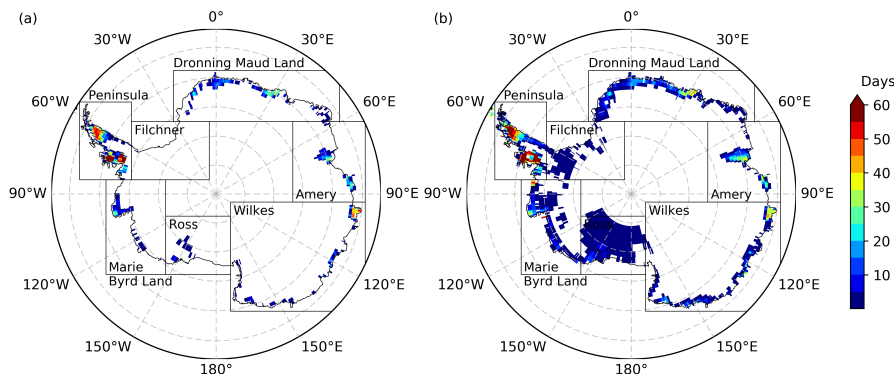
Figure 3. Annual mean of melting duration (days) from April 2010 to March 2018 detected with observations (a) at 1.4 GHz (SMOS) and (b) at 19 GHz (SSMIS). Seven regions are outlined.

Figure 3 shows the annual mean duration of melt season between April 2010 and March 2018 detected at both frequencies. Melting is concentrated on the coast with a maximum in the Antarctic Peninsula as previously reported for 19 GHz (Tedesco, 2009; Kuipers Munneke et al., 2012; Datta et al., 2018, 2019; Scott et al., 2019). The largest differences are observed in Filchner and Ross ice shelves where melt is detected to occur a few days every year at 19 GHz, but is insufficient to be detected at 1.4 GHz. The difference is certainly explained by the difference of sensitivity. Indeed, as these ice shelves only experience limited melt, the liquid water is likely concentrated in the uppermost few centimeters of the snowpack.

Figure 4 highlights that 19 GHz is more effective to detect short melting duration than 1.4 GHz. Indeed, more than 55% of the pixels where melt occurs remain wet for less than 10 days in a year according to 19 GHz observations, and about 20%
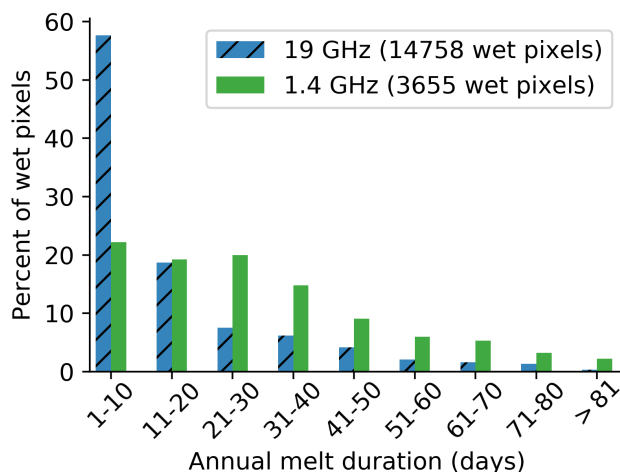
Figure 4. Annual melting duration distribution of wet pixels detected with 1.4 GHz (plain green) and 19 GHz (hatched blue).

remain wet between 11 and 20 days. At 1.4 GHz, the duration of the melt season is usually longer, in only 20% of the pixels
subject to melt, the season is 1-10 days, it is 11-40 days in 55% of the pixels. This hints that SMOS is only sensitive to long
and intense melt seasons.

5 Sensitivity to liquid water content

The sensitivity to liquid water at 1.4 GHz is investigated in order to understand the signal variations observed in Antarctica and
to investigate the observed differences with the 19 GHz melt detection.

5.1 Microwave emission modeling

T_B is simulated with the multi-layered Dense-Medium Radiative Theory model (DMRT-ML, Picard et al., 2013), available
online http://gp.snow-physics.science/dmrtml. This model is based on the radiative transfer theory (Tsang and Kong, 2001).
The snowpack is represented by a stack of snow horizontal layers defined by their thickness, temperature, density, grain size,
and liquid water content (LWC). Simulations are performed at 1.4 GHz and 19 GHz with an incidence angle of 55°.

A synthetic snowpack is assumed to run simulations. Its has a total thickness of 1000 m, and is divided in layers of 5 cm
from the surface to 500 m and 50 m below. Temperature is 273 K from the surface to 10 m depth, then constant at 263 K up
to 500 m depth and finally, linearly increasing to reach 273 K at the bottom. Density linearly increases from 300 kg m⁻³ at the
surface to 917 kg m⁻³ at 100 m in depth and is constant below (Leduc-Leballeur et al., 2015). Grain size is constant at 1 mm.
Picard et al. (2013) showed that grain size has an effect on the sensitivity to LWC at 19 GHz. Nevertheless, it is not expected
at 1.4 GHz because the wavelength is much larger than grain size and scattering by grains can be neglected (Mätzler, 1987).
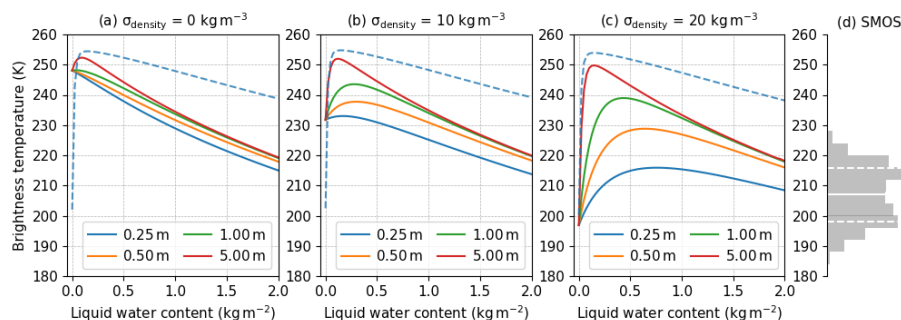
Figure 5. (a-c) DMRT-ML brightness temperature at H polarization (K) as a function of liquid water content for several wet snow thickness in the upper snowpack (colors) at 1.4 GHz (solid lines) and 0.25 m of wet snow at 19 GHz (dashed line) with three density variabilities (σ_{density}). (d) Daily winter SMOS observations distribution with mean (white solid) and standard deviation (white dashed).

5.2 Effect of snow density vertical variability

By modeling L-band emission at Dome C on the Antarctic Plateau, Leduc-Leballeur et al. (2015) highlighted that layering must be considered to obtain reliable T_B estimation. To assess if this is also the case for wet snow, the simulations are performed with a smooth density profile and two density profiles with an added Gaussian noise of standard deviation of 10 kg m^{-3} and 20 kg m^{-3}, respectively, between the surface and 300 m depth. Figure 5 shows the DMRT-ML simulations at both 1.4 GHz and 19 GHz as a function of LWC, and for various thicknesses of wet snow.

For the dry snowpack (LWC = 0 kg m^{-2}), the layering significantly decreases T_BH from 248.1 K for the smooth density profile to 231.8 K and 196.9 K for the density profiles with standard deviation 10 kg m^{-3} and 20 kg m^{-3}, respectively. In wet snow condition, the layering effect becomes weaker as the LWC increases and is insignificant (< 4 K variations) for LWC larger than 1 kg m^{-2} or when water is spread over a large thickness. Thus, between dry and wet conditions, T_BH difference increases with the layering.

Figure 5d shows daily SMOS T_BH from June to August – a period when snow is expected to be always dry – in 2010-2018. The histogram only includes pixels where melting has been detected at least once have been selected and where ice thickness is 1000±50 m to match with the snowpack configuration used for simulations. The SMOS T_BH average is 206.9±8.9 K. This suggests that simulations with a density variability lower than 10 kg m^{-3} overestimate the dry T_BH and thus underestimate the variations between dry and wet snow at 1.4 GHz. We thus now consider the case of a density variability of 20 kg m^{-3} only.

The simulations show that T_BH at 1.4 GHz increases from dry to wet by 19 K when the wet snow layer is 0.25 m and 53 K when it is 5 m (Figure 5c). While in both cases, the change is high and detectable, this highlights that not only the total column amount of liquid water is important but also the distribution in depth. Additionally, Figure 5c shows that the maximum of increase of T_BH is reached for LWC of 0.75 kg m^{-2} and 0.15 kg m^{-2}, respectively for the 0.25 m and 5 m thick wet snow layers. This means that the LWC sensitivity of 1.4 GHz T_BH is weaker when liquid water is confined in the uppermost tens of

centimeters of the snowpack. This is rational for choosing a lower first guess $a\sigma$ for the detection algorithm at 1.4 GHz than at the higher frequencies (Section 3).

Additionally, Figure 5c shows that regardless of the wet layer thickness, T_BH reaches a maximum at a certain LWC value,
150   which decreases when the wet layer becomes thicker. Thus, an increase in LWC is not detectable because of the T_B saturation. This jeopardizes the possibility of using microwave observations to estimate LWC values or even the wet layer thickness.

By contrast, at 19 GHz, the density variability has no effect and the T_BH variations are mainly driven by LWC. A sharp increase of 54 K is observed and the maximum is reach for LWC of $0.15\ \mathrm{kg\,m^{-2}}$. The thickness of the wet snow layer has no effect (not shown in Figure 5c).

155   As a conclusion, these simulations show that 19 GHz is more sensitive to liquid water than at 1.4 GHz and that other factors such as the vertical distribution of the water or the layering have a lesser influence. This indicates that detection of melt occurrence at the surface is more robust at 19 GHz.

5.3   Effect of the wet snow depth

We explore here the situation when the wet snow layer is buried under a layer of dry firn. This corresponds to the end of summer
160   when the snowpack freezes up from the surface, or on the ice shelves where melt water enters the crevasses and accumulates at depth. The simulations are performed with a wet snow layer ($0.2\ \mathrm{kg\,m^{-2}}$), progressively moved down from the surface to 400 m depth. The layer thickness is 1 m at 1.4 GHz and 0.1 m at 19 GHz to moderate the sensitivity effect presented in the previous section. Results highlight that T_BH is maximum when wet snow is at the surface for both frequencies and decreases within a few meters at 19 GHz and more gradually at 1.4 GHz (Figure 6). T_BH is still more than 10 K higher than in dry conditions
165   when the wet layer is at 60 m depth at 1.4 GHz. Deeper than 100 m, the difference between dry and wet T_BH is lower than 3 K, i.e. lower than the noise level with SMOS.

At 19 GHz, the simulation shows a T_BH variation of 2 K between dry and wet when the wet snow is at 5 m depth. Thus, the sensitivity to liquid water is relatively quickly lost at this frequency if the water percolate deep into the firn. However, observations at 19 GHz should still be suitable for the detection of remnant liquid water at the end of the season, and when the
170   snowpack is continuous, i.e. without crevasse.

These results suggest that despite a lower sensitivity at 1.4 GHz, liquid water could be detected with SMOS up to several tens of meters at depth and this is a new information compared to that provided by existing melt product derived from 19 GHz and higher frequencies observations. The difference observed between 19 GHz and 1.4 GHz could be exploited to determine if the melt event was limited to the few first centimeters of snowpack or if the event was produce a lot of water that percolated
175   over a sufficient thickness to be detected by SMOS.

Figure 7 maps the mean number of melting days detected at 1.4 GHz without concurrent detection at 19 GHz during summer season over our dataset. It shows that the geographical distribution is related to the total number of melt event (Figure 3), meaning that all the areas are concerned by the differential detection at both frequencies. On average, 10±8 days are detected only by SMOS. Moreover, over a total of about 117,000 melting days taking all pixels and summer seasons together detected
180   at 1.4 GHz, 28% are not concurrently detected at 19 GHz. These melting days happen on 1 February ± 23 days on average, i.e.
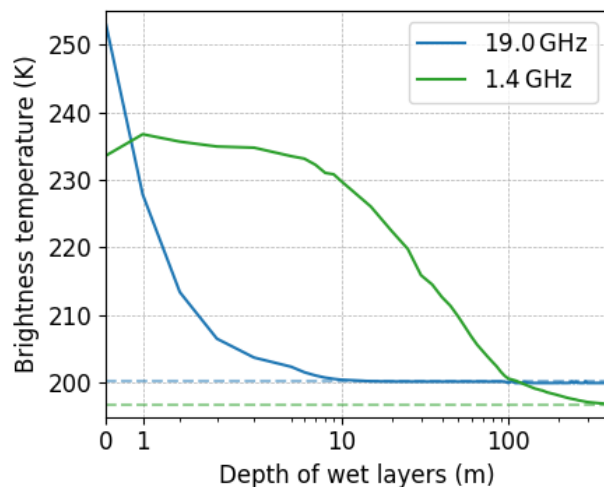
Figure 6. DMRT-ML brightness temperature at H polarization (K) for 55° of incidence angle as a function of the wet snow depth within the snowpack at 1.4 GHz (green) and 19 GHz (blue). Values for a dry snowpack are in dashed lines.
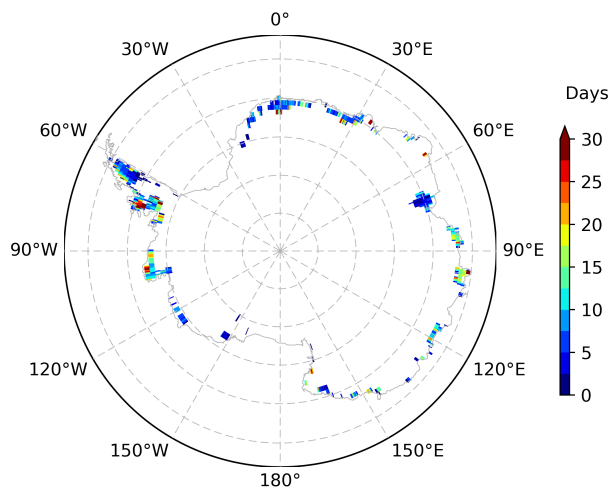
Figure 7. Mean melting days by summer season detected as melting at 1.4 GHz but dry at 19 GHz.

at the end of summer season. Conversely, over 225,000 melting days detected by 19 GHz during the same period, 66% are not concurrently detected at 1.4 GHz. This is in agreement with the difference of sensitivity between both frequencies suggested by the results of DMRT-ML simulations.

6 Conclusions

185 The L-band brightness temperature (T_B) from SMOS satellite has been explored to retrieve information about the melt season in Antarctica. Daily melt occurrence can be retrieved using previously developed algorithms for higher frequencies (Zwally and Fiegles, 1994; Torinesi et al., 2003) after a slight adaptation to account for the lower sensitivity at 1.4 GHz. The comparison of melt detected at 1.4 GHz and 19 GHz (Picard and Fily, 2006) shows a lower rate of detection at 1.4 GHz. In particular, SMOS misses short, probably weak, events, which are in contrast perfectly detected at 19 GHz.

190 A theoretical analysis has been performed using a snowpack emission radiative transfer model (DMRT-ML) in order to estimate the sensitivity of T_B at 1.4 GHz and 19 GHz to liquid water content (LWC) and water distribution in the snowpack. As expected from previous studies, a clear increase in T_B happens when snow becomes wet. However, the simulations clearly demonstrate that 1.4 GHz is less sensitive than 19 GHz, especially when liquid water stays within the first centimeters of the snowpack. A thick wet layer ($>$ about 0.5 m) is required to trigger a sharp and detectable T_B increase. Despite this limited 195 sensitivity, the simulations show that 1.4 GHz is suitable to detect wet snow buried under a dry surface. For instance, an increase in T_B higher than 10 K with respect to a dry snowpack can be observed with liquid water at up to 60 m depth according to the simulation configuration.

An avenue is a combined use of both frequencies to determine if a melt event was limited to the surface of snowpack or if it was intense enough to inject water at depth. However, further algorithmic work is needed to exploit this possibility of deep 200 water detection with SMOS.

Author contributions. MLL, GP and GM led the study and performed the analysis. AM and YHK supported for using the SMOS observations. All authors contributed to the manuscript.

Data availability. Daily occurrence of melt retrieved from SMOS available at www.catds.fr/Products/Available-products-from-CEC-SM/ CryoSMOS-project

205 *Competing interests.* The authors declare that they have no conflict of interest.

Acknowledgements. This study benefited from ESA support through the CryoSMOS project (contract 4000112262/14/I-NB) and the French space agency (CNES) support through the SMOS TOSCA project. SMOS L3 product comes from the CATDS, managed for the CNES by IFREMER (Brest, France).

References

210 Abdalati, W. and Steffen, K.: Snowmelt on the Greenland ice sheet as derived from passive microwave satellite data, Journal of Climate, 10, 165–175, https://doi.org/10.1175/1520-0442(1997)010<0165:SOTGIS>2.0.CO;2, 1997.

Al Bitar, A., Mialon, A., Kerr, Y., Cabot, F., Richaume, P., Jacquette, E., Quesney, A., Mahmoodi, A., Tarot, S., Parrens, M., Al-yaari, A., Pellarin, T., Rodriguez-Fernandez, N., and Wigneron, J.-P.: The Global SMOS Level 3 daily soil moisture and brightness temperature maps, Earth System Science Data, 9, 293–315, https://doi.org/10.5194/essd-9-293-2017, 2017.

215 Brodzik, M. J., Billingsley, B., Haran, T., Raup, B., and Savoie, M. H.: EASE-grid 2.0: Incremental but Significant Improvements for Earth-Gridded Data Sets, ISPRS International Journal of Geo-Information, 1, 32–45, https://doi.org/10.3390/ijgi1010032, 2012.

Brucker, L., Dinnat, E. P., Picard, G., and Champollion, N.: Effect of snow surface metamorphism on Aquarius L-band radiometer observations at Dome C, Antarctica, IEEE Trans. Geosci. Remote Sens., 52, 7408–7417, https://doi.org/10.1109/TGRS.2014.2312102, 2014.

Datta, R. T., Tedesco, M., Agosta, C., Fettweis, X., Kuipers Munneke, P., and van den Broeke, M.: Melting over the northeast Antarctic Penin-
220 sula (1999–2009): evaluation of a high-resolution regional climate model, Cryosphere (The), 12, 2901–2922, https://doi.org/10.5194/tc-12-2901-2018, 2018.

Datta, R. T., Tedesco, M., Fettweis, X., Agosta, C., Lhermitte, S., Lenaerts, J., and Wever, N.: The Effect of Foehn-Induced Surface Melt on Firn Evolution Over the Northeast Antarctic Peninsula, Geophysical Research Letters, 46, https://doi.org/10.1029/2018GL080845, 2019.

Golledge, N. R., Kowalewski, D. E., Naish, T. R., Levy, R. H., Fogwill, C. J., and Gasson, E. G.: The multi-millennial Antarctic commitment
225 to future sea-level rise, Nature, 526, 421, https://doi.org/10.1038/nature15706, 2015.

Jakobs, C. L., Reijmer, C. H., Kuipers Munneke, P., König-Langlo, G., and van den Broeke, M. R.: Quantifying the snowmelt–albedo feedback at Neumayer Station, East Antarctica, The Cryosphere, 13, 1473–1485, https://doi.org/10.5194/tc-13-1473-2019, 2019.

Kerr, Y. H., Waldteufel, P., Wigneron, J.-P., Martinuzzi, J., Font, J., and Berger, M.: Soil moisture retrieval from space: The Soil Moisture and Ocean Salinity (SMOS) mission, IEEE Trans. Geosci. Remote Sens., 39, 1729–1735, https://doi.org/10.1109/36.942551, 2001.

230 Kerr, Y. H., Waldteufel, P., Wigneron, J.-P., Delwart, S., Cabot, F., Boutin, J., Escorihuela, M.-J., Font, J., Reul, N., Gruhier, C., Juglea, S. E., Drinkwater, M. R., Hahne, A., Martín-Neira, M., and Mecklenburg, S.: The SMOS mission: New tool for monitoring key elements ofthe global water cycle, Proc. IEEE, 98, 666–687, https://doi.org/10.1109/JPROC.2010.2043032, 2010.

Kuipers Munneke, P., Picard, G., van den Broeke, M. R., Lenaerts, J. T. M., and van Meijgaard, E.: Insignificant change in Antarctic snowmelt volume since 1979, Geophysical Research Letter, 39, https://doi.org/10.1029/2011GL050207, 2012.

235 Leduc-Leballeur, M., Picard, G., Mialon, A., Arnaud, L., Lefebvre, E., Possenti, P., and Kerr, Y.: Modeling L-band brightness temperature at Dome C in Antarctica and comparison with SMOS observations, IEEE Trans. Geosci. Remote Sens., 53, 4022–4032, https://doi.org/10.1109/TGRS.2015.2388790, 2015.

Leduc-Leballeur, M., Picard, G., Macelloni, G., Arnaud, L., Brogioni, M., Mialon, A., and Kerr, Y.: Influence of snow surface properties on L-band brightness temperature at Dome C, Antarctica, Remote Sensing of Environment, 199, 427–436,
240 https://doi.org/10.1016/j.rse.2017.07.035, 2017.

Liu, H., Wang, L., and Jezek, K. C.: Wavelet-transform based edge detection approach to derivation of snowmelt onset, end and duration from satellite passive microwave measurements, International Journal of Remote Sensing, 26, 4639–4660, 2005.

Liu, H., Wang, L., and Jezek, K. C.: Spatiotemporal variations of snowmelt in Antarctica derived from satellite scanning multichannel microwave radiometer and Special Sensor Microwave Imager data (1978–2004), Journal of Geophysical Research: Earth Surface, 111,
245 https://doi.org/10.1029/2005JF000318, 2006.

Maslanik, J. and Stroeve, J.: DMSP SSM/I-SSMIS Daily Polar Gridded Brightness Temperatures, Version 4., NASA National Snow and Ice Data Center Distributed Active Archive Center, Boulder, Colorado, USA, https://doi.org/10.5067/AN9AI8EO7PX0, 2004, updated 2018.

Mätzler, C.: Applications of the interaction of microwaves with the natural snow cover, Remote sens. rev., 2, 259–387, https://doi.org/10.1080/02757258709532086, 1987.

250 Mote, T. L., Anderson, M. R., Kuivinen, K. C., and Rowe, C. M.: Passive microwave-derived spatial and temporal variations of summer melt on the Greenland ice sheet, Annals of Glaciology, 17, 233–238, https://doi.org/10.3189/S0260305500012891, 1993.

Passalacqua, O., Picard, G., Ritz, C., Leduc-Leballeur, M., Quiquet, A., Larue, F., and Macelloni, G.: Retrieval of the Absorption Coefficient of L-Band Radiation in Antarctica From SMOS Observations, Remote Sensing, 10, 1954, https://doi.org/10.3390/rs10121954, 2018.

Picard, G. and Fily, M.: Surface melting observations in Antarctica by microwave radiometers: Correcting 26-year time series from changes
255 in acquisition hours, Remote Sens. Environ., 104, 325–336, https://doi.org/10.1016/j.rse.2006.05.010, 2006.

Picard, G., Fily, M., and Gallée, H.: Surface melting derived from microwave radiometers: a climatic indicator in Antarctica, Ann. Glaciol., 46, 29–34, 2007.

Picard, G., Brucker, L., Roy, A., Dupont, F., Fily, M., Royer, A., and Harlow, C.: Simulation of the microwave emission of multi-layered snowpacks using the Dense Media Radiative transfer theory: the DMRT-ML model, Geosci. Model Dev., 6, 1061–1078,
260 https://doi.org/10.5194/gmd-6-1061-2013, 2013.

Ridley, J.: Surface melting on Antarctic Peninsula ice shelves detected by passive microwave sensors, Geophysical Research Letters, 20, 2639–2642, https://doi.org/10.1029/93GL02611, 1993.

Scambos, T. A., Hulbe, C., Fahnestock, M., and Bohlander, J.: The link between climate warming and break-up of ice shelves in the Antarctic Peninsula, Journal of Glaciology, 46, 516–530, https://doi.org/10.3189/172756500781833043, 2000.

265 Scott, R. C., Nicolas, J. P., Bromwich, D. H., Norris, J. R., and Lubin, D.: Meteorological drivers and large-scale climate forcing of West Antarctic surface melt, Journal of Climate, 32, 665–684, 2019.

Surdyk, S.: Using microwave brightness temperature to detect short-term surface air temperature changes in Antarctica: An analytical approach, Remote Sens. Environ., 80, 256–271, https://doi.org/10.1016/S0034-4257(01)00308-X, 2002.

Tedesco, M.: Snowmelt detection over the Greenland ice sheet from SSM/I brightness temperature daily variations, Geophysical Research
270 Letters, 34, https://doi.org/10.1029/2006GL028466, 2007.

Tedesco, M.: Assessment and development of snowmelt retrieval algorithms over Antarctica from K-band spaceborne brightness temperature (1979–2008), Remote Sensing of Environment, 113, 979–997, https://doi.org/10.1016/j.rse.2009.01.009, 2009.

Tedesco, M., Abdalati, W., and Zwally, H.: Persistent surface snowmelt over Antarctica (1987–2006) from 19.35 GHz brightness temperatures, Geophysical Research Letters, 34, https://doi.org/10.1029/2007GL031199, 2007.

275 Torinesi, O., Fily, M., and Genthon, C.: Variability and trends of the summer melt period of Antarctic ice margins since 1980 from microwave sensors, Journal of Climate, 16, 1047–1060, 2003.

Tsang, L. and Kong, J. A.: Scattering of Electromagnetic Waves, vol.3: Advanced Topics, Wiley Interscience, 2001.

von Storch, H. and Zwiers, F. W.: Statistical analysis in climate research, Cambridge University Press, 2001.

Zwally, J. H. and Fiegles, S.: Extent and duration of Antarctic surface melting, Journal of Glaciology, 40, 463–475,
280 https://doi.org/10.3198/1994JoG40-136-463-375, 1994.